Folding Kinetics of Villin 14T, a Protein Domain with a Central β-Sheet and Two Hydrophobic Cores†

Sung E. Choe,‡ Paul T. Matsudaira,§ John Osterhout,|| Gerhard Wagner,⊥ and Eugene I. Shakhnovich*,@

Committee on Higher Degrees in Biophysics, Harvard University, Boston, Massachusetts 02115, Whitehead Institute for Biomedical Research, Massachusetts Institute of Technology, Cambridge, Massachusetts 02142, Rowland Institute for Science, Cambridge, Massachusetts 02142, Department of Biological Chemistry and Molecular Pharmacology, Harvard Medical School, Boston, Massachusetts 02115, and Department of Chemistry, Harvard University, Cambridge, Massachusetts 02138

Received April 20, 1998; Revised Manuscript Received August 6, 1998

ABSTRACT: The thermodynamics and kinetics of folding are characterized for villin 14T, a 126-residue protein domain. Equilibrium fluorescence measurements reveal that villin 14T unfolds and refolds reversibly. The folding kinetics was monitored using stopped-flow with fluorescence and quenched-flow with NMR and mass spectrometry. Unfolding occurs in a single-exponential phase in the stopped-flow experiments, and about 75% of the total amplitude is recovered in the fast phase of refolding. The remaining 25% of the amplitude probably represents trapping in cis−trans proline isomerization pathways. At 25 °C, the stability estimate obtained by extrapolation from the transition region of the stopped-flow chevron matches the stability value from equilibrium urea titrations (ΔG = 9.7 kcal/mol, m value = 2.2 kcal mol^{-1} M^{-1}). At low final urea concentrations, however, the refolding kinetics deviates from the two-state model, indicating the formation of an intermediate. Under these conditions, quenched-flow followed by NMR and mass spectrometry show no detectable hydrogen-bonded intermediate in the fast refolding phase. In contrast, agreement is observed between the equilibrium and kinetic estimates of stability at 37 °C (ΔG = 6.0 kcal/mol, m value = 1.6 kcal mol^{-1} M^{-1}), at all observed urea concentrations, demonstrating apparent two-state folding at this temperature. This result shows that the two-state folding model, previously applied to small domains with single, central hydrophobic cores, can also describe the folding of a larger domain with multiple core structures.

Many polypeptides fold spontaneously to their native states from a random coil conformation (*1*). This folding ability contradicts Levinthal's observation that an unfolded polypeptide has too many conformational degrees of freedom to fold in a reasonable time, assuming a random search mechanism (*2*). Therefore, protein folding should not occur through random search; the accessible conformational space must be restricted during folding. Many studies have been devoted to characterizing folding pathway(s) for different proteins.

The Levinthal paradox could be resolved if proteins fold through discrete metastable intermediates, which would reduce the number of accessible states during folding. Kinetic intermediates have been observed during the folding of many proteins (*3*−*13*). However, it is unknown in most cases whether intermediate formation is an obligatory step, or actually serves as a kinetic trap. These two alternatives can be distinguished by studying the kinetics at short refolding times. An initial delay in native state formation, during which time the intermediate accumulates, would indicate the presence of an obligatory intermediate (*14*, *15*). In contrast, if some molecules reach the native state before the intermediate can accumulate, then intermediate formation acts as a kinetic trap. The latter case is observed in lysozyme (*16*), which folds through two parallel pathways, a fast pathway (50 ms) to the native state and a slow pathway (420 ms) to a kinetically trapped intermediate (*5*, *11*, *16*). The fast pathway does not require a metastable folding intermediate (*16*), implying that the accumulation of intermediates is not a general solution to the Levinthal paradox.

In addition, 10−15 small proteins fold without any detectable intermediates, in an apparent two-state manner (*17*−*24*). These proteins show agreement between equilibrium and kinetic measurements of ΔG_{NU} (free energy of unfolding) and m value (slope of the ΔG_{NU} vs denaturant concentration plot) (*20*). Since intermediates do not accumulate in these cases, they do not serve to restrict the accessible conformational space, and therefore cannot explain the Levinthal paradox. As an alternative, authors propose a nucleation mechanism for two-state folding, in which the formation of a subset of native contacts ("nucleus") is the rate-limiting step, followed by direct folding to the native state (*25*, *26*).

Intermediate accumulation frequently depends on the environmental conditions, indicating the diversity of possible folding pathways for a single protein, as well as between different proteins. Kinetic intermediates often appear or disappear as the result of changing variables such as

† This work was supported by NIH Grants GM52126 to E.I.S., GM38608 to G.W., and GM52703 to P.T.M.

* To whom correspondence should be addressed.
‡ Committee on Higher Degrees in Biophysics, Harvard University.
§ Massachusetts Institute of Technology.
|| Rowland Institute for Science.
⊥ Harvard Medical School.
@ Department of Chemistry, Harvard University.

S0006-2960(98)00889-7 CCC: $15.00
Published on Web 09/25/1998

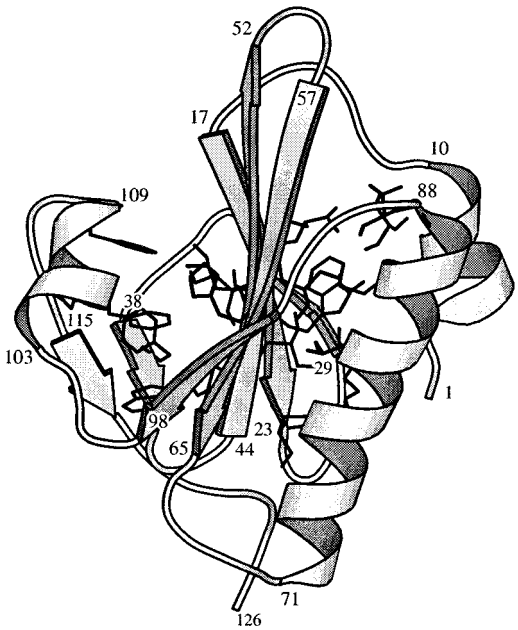

FIGURE 1: Cartoon of villin 14T, based on the solution structure by Markus et al. (*34*, *35*). Side chains constituting the two hydrophobic cores on either side of the central β-sheet are shown. The left hydrophobic core is mostly aromatic, while the right core is primarily aliphatic. When only side chain heavy atoms are considered, the minimum separation distance between the two cores is 5.2 Å [between the two atom pairs Y45 (CD1) and C44 (CB), and I20 (CB) and W21 (CE3)]. This figure was generated using the program MolScript (*54*).

temperature, denaturant concentration, and pH. For example, a folding intermediate of F45W ubiquitin is detectable at 25 °C, but not at 8 °C (*27*). Many proteins show a folding intermediate at low denaturant concentrations, but reveal apparent two-state folding behavior near the transition midpoint of the denaturant titration curve (*27*−*29*). At high pH, cytochrome *c* folds with a misligated heme intermediate, which becomes undetectable below pH 5 (*13*, *30*−*32*). Therefore, the protein folding energy landscape is highly sensitive to experimental conditions; such patterns of sensitivity can provide valuable information about any involved intermediate(s).

We are interested in the folding kinetics of villin 14T, a 126-residue domain with almost ideal properties for studying protein folding under a wide range of experimental conditions. Villin 14T is the N-terminal domain of chicken villin, which belongs to a superfamily of homologous actin bundling and/or severing proteins (*33*). This domain is stable under a wide range of pHs and salt concentrations, and can be purified with high yields from *Escherichia coli*. Villin 14T contains two tryptophan residues, three trans prolines, and no disulfide bonds. The solution structure of villin 14T has been solved and refined (*34*, *35*), showing a fold distinctive for this superfamily, consisting of a five-stranded central β-sheet, flanked on one side by two α-helices and on the other side by a short helix and a two-stranded β-sheet (Figure 1). Two hydrophobic cores, one consisting primarily of aromatic side chains and the other predominantly filled with aliphatic side chains, stabilize the interactions between the central β-sheet and adjacent secondary structures. The kinetics of folding to this protein topology has not been previously studied.

To study how folding behavior can be modulated by the experimental conditions, the folding kinetics of villin 14T was monitored using stopped-flow with fluorescence and quenched-flow followed by NMR[1] and mass spectrometry. At 25 °C and in urea, the protein folds in a two-state manner near the transition region, but seems to involve a refolding intermediate at low final urea concentrations. Quenched-flow experiments reveal that at low urea concentrations, the fast refolding phase does not involve a stably hydrogen-bonded intermediate. At 37 °C, villin 14T folds in a two-state manner at all measured urea concentrations. The 37 °C data are the first demonstration of apparent two-state folding for a domain with multiple core structures (central β-sheet and two hydrophobic cores). However, as shown by the data at 25 °C, the two-state behavior at 37 °C is highly dependent on the environmental conditions.

EXPERIMENTAL PROCEDURES

Materials. Ultrapure-grade guanidine hydrochloride (GuHCl) was purchased from ICN Biochemicals, and deuterium oxide was obtained from Cambridge Isotope Laboratory. ^{15}N-labeled ammonium chloride was obtained from Isotec, Inc.

Expression and Purification of Villin 14T. Villin 14T was expressed from BL21(DE3) *E. coli* cells transformed with the villin 14T/pAED4 vector (*36*). For unlabeled preparations, overnight cultures were grown in LB broth with ampicillin (100 mg/L); for ^{15}N-labeled proteins, cells were grown in minimal M9 medium [with $^{15}NH_4Cl$, and supplemented with 2 mM $MgSO_4$, 0.1 mM $CaCl_2$, 0.005% (w/v) thiamine hydrochloride, 100 mg/L ampicillin, and 0.4% (w/v) glucose], with IPTG induction at $A_{600} = 0.6$. One liter culture growths were harvested by centrifugation, and cell pellets were stored at −20 °C until further use. Cell pellets were gently resuspended in 25 mL (4 °C) of lysis buffer [50 mM Tris (pH 8), 20 mM NaCl, 2 mM EDTA, and 2 mM DTT], lysed using a French press, sonicated for 1 min, and then centrifuged for 40 min at 39000*g* (4 °C). The resulting supernatant was loaded onto a 40 mL DEAE column, which had been equilibrated at 4 °C with "DEAE buffer" [10 mM Tris (pH 8) and 100 mM NaCl]. (All columns were operated with gravity flow, at nearly maximal flow rates.) All flow-through was collected, and the column was washed with DEAE buffer until A_{280} approached the baseline. The flow-through was then diluted with 15 mM Mes (pH 5.85 and 4 °C) to 3 times the original volume; the resulting pH was checked (should be 6.0−6.1). This diluted flow-through was then loaded onto a 40 mL CM column, which was pre-equilibrated at 4 °C with "CM buffer" [10 mM Mes (pH 6) and 30 mM NaCl]. After loading, the column was washed with more CM buffer until A_{280} reached the baseline. Villin 14T was eluted from the column by applying a 30 to 300 mM NaCl gradient, over 300 mL [buffer was 10 mM Mes (pH 6)]. Collected fractions were checked using SDS−PAGE, pooled, dialyzed overnight into Milli-Q H_2O, and lyophilized. An extinction coefficient of 22 900 OD_{280}/M

[1] Abbreviations: GuHCl, guanidine hydrochloride; CI2, chymotrypsin inhibitor 2; βME, β-mercaptoethanol; MALDI-TOF, matrix-assisted laser desorption ionization time-of-flight; NMR, nuclear magnetic resonance; HSQC, heteronuclear single-quantum coherence; IPTG, isopropyl thio-β-D-galactoside; EDTA, ethylenediaminetetraacetate; DTT, dithiothreitol.

was used to determine protein concentrations. The yield for unlabeled preps was 150 mg/L of cells and, for ^{15}N-labeled preps, 40−60 mg/L of cells.

Equilibrium Fluorescence Measurements. A Hitachi F-4500 fluorimeter was used to obtain an equilibrium unfolding curve for villin 14T. To generate a urea titration, two buffers were prepared, each containing 1 μM villin 14T, 50 mM acetic acid, 15 mM NaCl, and 1 mM βME (pH 4.1); one buffer contained 0 M urea, while the other contained 7.5 M urea. The buffer with 0 M urea served as the first sample. Successive samples with increasing urea concentrations were generated by replacing a volume of the previous sample with the same volume of the 7.5 M urea buffer. The fluorescence level of each sample was obtained by exciting at 295 nm and measuring the emission at 320 nm. The bandwidth for excitation was 2.5 nm, while that for emission was 10 nm. Each data point was the fluorescence signal averaged over 60 s. A 1 cm × 4 mm quartz cuvette with a stir bar was used.

Stopped-Flow with Fluorescence. The kinetics of villin 14T refolding and unfolding was studied using an Applied Photosystems SX-17MV stopped-flow fluorescence apparatus, thermostated at 25 and 37 °C. For all stopped-flow experiments, "buffer A" was mixed with "buffer B" in a 1:5 ratio to generate the desired denaturant jump. For refolding experiments, buffer A contained 2.5 μM villin 14T, 6.5 M urea, 50 mM acetic acid, 15 mM NaCl, and 1 mM βME (pH 4.1); buffer B contained 50 mM acetic acid, 15 mM NaCl, 1 mM βME (pH 4.1), and a range of urea concentrations. In the unfolding experiments, buffer A contained 2.5 μM villin 14T, 3 M urea, 50 mM acetic acid, 15 mM NaCl, and 1 mM βME (pH 4.1), and buffer B contained 50 mM acetic acid, 15 mM NaCl, 1 mM βME (pH 4.1), and a range of urea concentrations. The refractive index was measured to verify the urea concentrations of all buffers (*37*). Upon mixing, the fluorescence was monitored by exciting at 280 nm, and detecting all emission above 300 nm. The dead time of the stopped-flow apparatus was ∼5 ms. Resulting kinetic traces were fitted to single-exponential curves.

Quenched-Flow with NMR. Quenched-flow experiments were performed using a Biologic QFM-5 rapid mixing module, operated at room temperature (∼21 °C). The following is a modification of a previously published protocol (*17*).

For refolding in 2.4 M urea, the lyophilized, ^{15}N-labeled protein was first dissolved (to 40 μM) in 6.5 M urea, 50 mM acetic acid, 15 mM NaCl, and 1 mM DTT (pH 4.1) in D_2O (reading unadjusted for isotope effect). This buffer was mixed in a 1:12 ratio with 50 mM acetic acid, 15 mM NaCl, and 2.06 M urea (pH 4.1) in H_2O, to produce a refolding environment of 3 μM protein, 2.4 M urea, and pH 4.1. Delays for monitoring the time course of refolding ranged from 6 to 340 ms. To initiate amide hydrogen exchange, the buffer was mixed in a 13:12 ratio with 180 mM glycine and 15 mM NaCl (pH 9.8). The resulting pH was 9.3, which promotes rapid H−D exchange ($\tau = 0.6$ ms). The exchange delay was 20 ms. Exchange was quenched by addition in a 25:9 ratio of 1.5 M acetic acid and 15 mM NaCl. The final pH was 3.7, essentially stopping exchange of all interior amides. The product was collected, concentrated to 250 μL using Amicon centripreps and centricons (molecular mass cutoff of 3 kDa), and then dialyzed overnight into NMR buffer [50 mM NaH_2PO_4 and 100 mM NaCl (pH 4.1)]. Samples were adjusted to 10% D_2O before acquiring heteronuclear single-quantum coherence spectra (Bruker AMX500 NMR instrument). After peak volumes were calculated using the Felix95 analysis package, they were then renormalized to adjust for differences in sample concentration. An all-protonated sample was used as the 0 ms time point, and all volumes reported here are fractions of the corresponding peak volume from the 0 ms sample.

Quenched-Flow with Mass Spectrometry. For analysis of refolding populations using mass spectrometry (*38*), quenched-flow mixing was repeated under the same conditions as above, using 1 μM unlabeled protein and 2.3 M urea during the refolding phase. To optimize the resolution of the mass spectrum, the mixing product was collected, concentrated 100-fold using Amicon centricons and centripreps, and dialyzed overnight into Milli-Q H_2O. A PerSeptives Voyager-Elite Biospectrometry workstation [matrix-assisted laser desorption ionization time-of-flight (MALDI-TOF)] was used to acquire mass spectra. Each sample was prepared by mixing on the target 1 μL of sample with 1 μL of matrix (70% acetonitrile, 20 mg/mL sinapinic acid, and 0.1% trifluoroacetic acid), immediately drying the mixture by blowing gaseous N_2 over the target, and then directly placing the target in the spectrometer. Spectra were acquired using the following parameters: accelerating voltage of 25 000 V, grid voltage of 91%, guide wire voltage of 0.1%, and 50 000 channels (4 ns). Mass values were calibrated using commercially purified horse heart cytochrome *c* and horse heart myoglobin as standards.

RESULTS

Equilibrium Results. At 25 and 37 °C, urea titrations of villin 14T monitored by fluorescence show a cooperative unfolding transition between 3 and 5 M urea (Figure 2A,B). The equilibrium constant (K) is estimated from the fluorescence data using

$$K = (F_n - F)/(F - F_u)$$

where F_n is the fluorescence of the native state and F_u is the unfolded state fluorescence. A linear dependence of F_n and F_u on urea concentration is assumed. The equilibrium free energy difference between the folded and unfolded states is calculated ($\Delta G = -RT \ln K$). ΔG is then fitted as a linear function of urea concentration within the transition region:

$$\Delta G(C) = \Delta G(0) + mC$$

where C is the urea concentration and m is the slope of the $\Delta G(C)$ versus C graph (*37*). The m value correlates with the extent of protein surface burial upon folding (*39*), and roughly indicates the degree of cooperativity of folding. The resulting fitted parameters are given in Table 1. At 25 °C, $\Delta G(0) = 9.8 \pm 0.1$ kcal/mol and $m = 2.32 \pm 0.02$ kcal mol^{-1} M^{-1}, while at 37 °C, $\Delta G(0) = 6.2 \pm 0.1$ kcal/mol and $m = 1.59 \pm 0.04$ kcal mol^{-1} M^{-1}. Unfolding by chemical denaturation is reversible, and refolding occurs within the 20 s dead time of a hand-mixing experiment. Thermal unfolding was also observed using circular dichroism at 280 nm. Villin 14T unfolds cooperatively at about 65 °C, but this transition is not reversible under the observed conditions.

Table 1: Comparison of Equilibrium and Kinetic Parameters

Equilibrium: Fluorescence Titration[a]

denaturant	T (°C)	$\Delta G(0)$ (kcal/mol)	m (kcal mol^{-1} M^{-1})
urea	25	9.8 ± 0.1	2.32 ± 0.02
urea	37	6.2 ± 0.1	1.59 ± 0.04
GuHCl	25	9.8 ± 0.1	3.93 ± 0.03

Kinetics: Stopped-Flow with Fluorescence[b]

denaturant	T (°C)	$\Delta G_{kin}(0)$ (kcal/mol)	m_{kin} (kcal mol^{-1} M^{-1})
urea	25	9.5 ± 0.6	2.1 ± 0.1
urea	37	5.9 ± 0.2	1.5 ± 0.1
GuHCl	25	5.5 ± 0.2	2.5 ± 0.1

Kinetics: Other Fitted Parameters from Stopped-Flow with Fluorescence Experiments[b]

denaturant	T (°C)	ln[$k_f(0)$] [$k_f(0)$ in s^{-1}]	m_f (kcal mol^{-1} M^{-1})	ln[$k_u(0)$] [$k_u(0)$ in s^{-1}]	m_u (kcal mol^{-1} M^{-1})
urea	25	11.9 ± 0.6	−1.8 ± 0.1	−4.1 ± 0.2	0.33 ± 0.02
urea	37	6.8 ± 0.1	−1.11 ± 0.02	−2.8 ± 0.2	0.41 ± 0.03
GuHCl	25	7.5 ± 0.2	−1.8 ± 0.1	−1.8 ± 0.2	0.69 ± 0.03

[a] $\Delta G(0)$ and m are the equilibrium parameters obtained from the data in Figures 2 and 6A (see Figure 2 for the fitted equation). [b] Values for ln[$k_f(0)$], m_f, ln[$k_u(0)$], and m_u were fitted from the stopped-flow chevrons in Figures 4 and 7B (Figure 4 describes the fitted equation). The values of $\Delta G_{kin}(0)$ and m_{kin} predicted from kinetics were then calculated using $\Delta G_{kin}(0) = -RT \ln[k_u(0)/k_f(0)]$ and $m_{kin} = m_u - m_f$, respectively.

Stopped-Flow with Fluorescence. Rapid mixing followed by fluorescence measurement indicates the level of tryptophan burial during folding and unfolding. Example kinetic traces are shown in Figure 3. All of the unfolding curves fit well to single-exponential equations. Refolding kinetics consists of a fast phase whose amplitude of fluorescence change is 73% of that during unfolding (inset of Figure 4A). Only the fast phase is considered here; the remaining 27% of the amplitude is assumed to be the result of cis−trans proline isomerization. Further analysis will be necessary to determine if this assumption is valid. However, the slow refolding phases of CI2 (23% amplitude) and tendamistat (20% amplitude) have been attributed to proline isomerization; CI2 contains four trans prolines in the native state, while Tendamistat contains three (*23*, *40*). Since villin 14T contains three trans prolines in the native state, it would be similar to the previous reports if 27% of the refolding amplitude is the result of proline isomerization.

At 25 °C, there is a linear dependence of the log of the rate constant (k_f or k_u) with urea concentration in the region of 3.4−8 M urea (Figure 4A):

$$\ln[k_f(C)] = \ln[k_f(0)] + (m_f/RT)C$$

and

$$\ln[k_u(C)] = \ln[k_u(0)] + (m_u/RT)C$$

where C is the final urea concentration, $k_f(C)$ and $k_u(C)$ are the refolding and unfolding rate constants as a function of C, respectively, and m_f and m_u represent the dependence of ln(k_f) and ln(k_u) on C, respectively. At 25 °C, ln(k) values deviate from the fitted line at low urea concentrations (<3.4 M urea), indicating departure from two-state behavior in this region. At 37 °C, the ln($k_{f,u}$) vs urea concentration graph remains linear at all observed urea concentrations (Figure 4B). Fitted values for ln[$k_f(0)$], ln[$k_u(0)$], m_f, and m_u at 25 and 37 °C are given in Table 1.

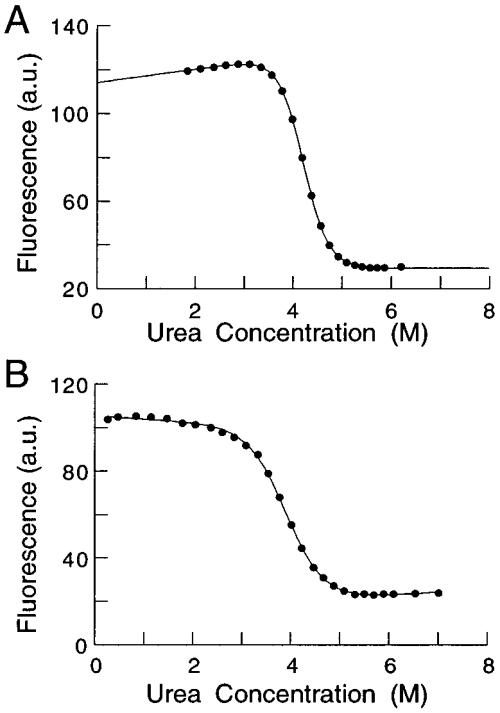

FIGURE 2: Equilibrium unfolding of villin 14T monitored with fluorescence. Lines represent the fit of the data to the equation $y = [(a + bx) + (c + dx) \exp[-[\Delta G(0) + mx]/RT]]/[1 + \exp[-[\Delta G(0) + mx]/RT]]$, where y is the fluorescence, x is the denaturant concentration, $a + bx$ is the fluorescence of the native state, and $c + dx$ is the fluorescence of the unfolded state. (A) Urea titration at 25 °C and (B) urea titration at 37 °C.

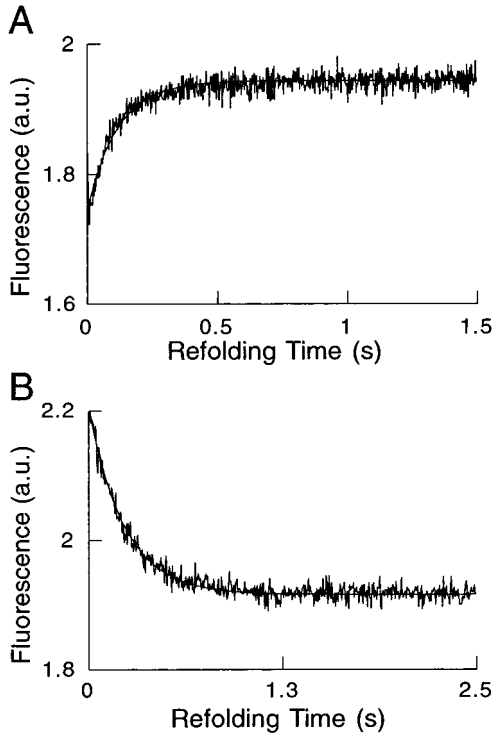

FIGURE 3: Representative folding (A) and unfolding (B) traces from stopped-flow fluorescence in urea, at 25 °C. The curve represents the best fit of the data to a single-exponential equation with a nonzero end point.

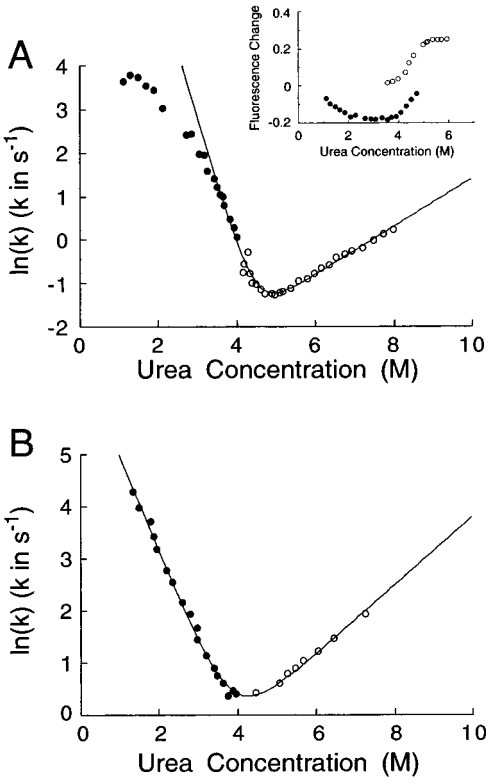

FIGURE 4: Stopped-flow fluorescence data in urea, in ln(k) vs denaturant concentration plots. Filled circles represent folding data, and unfilled circles represent unfolding data. Data points were fitted to $y = \ln[\exp[\ln[k_f(0)] + m_f x] + \exp[\ln[k_u(0)] + m_u x]]$, where $y = \ln(k_{obs})$ and x is the denaturant concentration. The line shows the resulting fit. (A) In urea, at 25 °C. For this chevron, only the data points above 3.4 M urea were used for the fitting. The inset depicts the change in fluorescence upon folding (●) or unfolding (○), as a function of the final urea concentration. (B) In urea, at 37 °C. All data points were used for fitting.

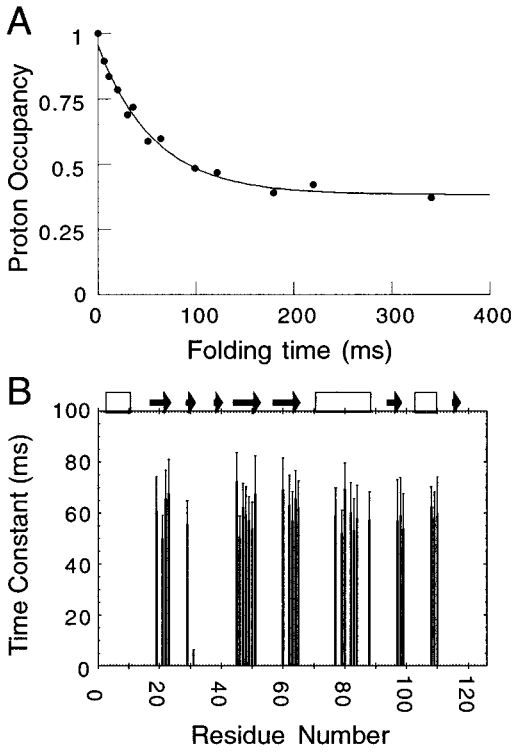

FIGURE 5: Quenched-flow followed by NMR, in 2.4 M urea, at 21 °C. (A) Representative time course of protection for residue 84. (B) Time constants for the 31 amides studied (residues 19, 21−23, 29, 31, 45−51, 60, 62−65, 77, 79, 80, 82−84, 88, 97−99, and 108−110). Secondary structure elements are indicated above the graph; boxes are helices, and arrows are β-strands.

At 25 °C, the fast phase amplitude during refolding decreases as the final urea concentration is lowered (inset of Figure 4A), which is the result of an increasing fluorescence signal right after mixing (data not shown). This suggests that the tryptophans (and other aromatic residues) are partly buried within the dead time of the experiment, at low final urea concentrations. At 37 °C, the fast phase amplitude does not significantly decrease with lower urea concentrations (data not shown).

Comparison of Stopped-Flow Kinetics with Equilibrium. The free energy of unfolding at zero denaturant concentration can be estimated from the above kinetic data:

$$\Delta G_{kin}(0) = -RT \ln[k_u(0)/k_f(0)]$$

Values of $\Delta G_{kin}(0)$ are shown in Table 1. At 25 °C, $\Delta G_{kin}(0) = 9.5 \pm 0.6$, and at 37 °C, $\Delta G_{kin}(0) = 5.9 \pm 0.2$; these correspond within error to $\Delta G(0)$ values derived from equilibrium experiments. Similarly, an m value can be predicted using kinetics data ($m_{kin} = m_u - m_f$). At 25 °C, $m_{kin} = 2.1 \pm 0.1$ kcal mol^{-1} M^{-1}, while at 37 °C, $m_{kin} = 1.5 \pm 0.1$ kcal mol^{-1} M^{-1}. These values also agree with the m values obtained from the equilibrium data (Table 1). The $\Delta G_{kin}(0)$ and m_{kin} values at 25 °C are obtained by extrapolating the data from the 3.4−8.0 M urea region of the stopped-flow chevron. Since there is significant rollover of the chevron plot below 3.4 M urea at 25 °C, the agreement of kinetic data with equilibrium stability and the m value does not apply below 3.4 M urea.

Quenched-Flow Experiments with Urea. Quenched-flow mixing followed by NMR and mass spectrometry was performed to determine whether the intermediate suggested by the stopped-flow data at 25 °C includes stabilized hydrogen-bonded structure. The results show that there is no such stable hydrogen bonding in the intermediate. Protection of amides from exchange with solvent is monitored during refolding at 2.4 M urea, at which concentration there is a clear deviation of the stopped-flow chevron from two-state behavior. Of the 126 backbone amides, 31 exchange slowly enough from the native state so that they can be studied by this technique. The resulting refolding traces fit well to single exponentials decaying to non-zero end points (e.g., Figure 5A). Thirty out of 31 probes show approximately the same time constant for refolding ($\tau \approx 60$ ms), with an amplitude of about 65% (Figure 5B). The stopped-flow fluorescence experiment also shows a 60 ms refolding time constant in 2.4 M urea, suggesting that the protection of amides observed in this experiment is due to the formation of native structure, and not the formation of an intermediate. The remaining 35% of the proton signal does not decay during the first 340 ms of refolding, which is the maximum refolding time studied in this experiment (Figure 5A). The only exception to the uniform protection kinetics of the amide probes is V31. This amide seems to become protected with a time constant of 5 ms. It is difficult to rationalize that this residue is part of a folding core; its fast protection kinetics can be better explained by local stiffness. Both residues 30 and 32 are prolines, implying

that this region is relatively rigid. V31 is on the protein surface in the native state, and the amide of V31 makes a hydrogen bond with the carbonyl oxygen of V29, implying that the protection of V31 from H−D exchange is indicative more of local rigidity than of overall protein folding.

The above quenched-flow mixing was repeated with unlabeled protein to observe the mass distribution changes due to amide hydrogen deuteration during refolding, using mass spectrometry. At zero refolding time, all protein molecules are unfolded, and therefore, all amide deuteriums exchange with H_2O during the high-pH pulse, resulting in a single peak at the all-proton position. (In fact, there is a slight shift in the all-proton position because of the residual deuterium component during the high-pH pulse.) At intermediate folding times, if some of the molecules have completely folded, all their internal amides (31 of them) are protected against exchange with H_2O, and remain deuterated in the final product; thus, there should be a peak at the mass of the protonated protein plus the number of internal amides. In contrast, if some of the proteins partially fold at intermediate times, one would expect to see a peak between the fully folded and unfolded positions. The data in Figure 6A show that the refolding reaction mixture contains no intermediates with stable hydrogen bonding. Although the spectra do not give fully resolved peaks, there are only two peak positions as determined by double-Gaussian fitting. The all-proton mass of villin 14T is 14 158 Da. One peak is near the location of the all-protonated (unfolded) protein (14 162 Da), and the other peak is 28 Da away (about 14 186 Da), which is approximately the number of nonexchanging internal amide hydrogens in this experiment, and therefore corresponds to the fully folded protein. Small variations in the peak positions (≈3−4 Da) are within experimental error. To measure the time course of the folding reaction, the fitted double-Gaussian curves were integrated to calculate the fraction of unfolded molecules at each time point. A plot of the unfolded fraction as a function of time is shown in Figure 6B. Fitting of this plot to a single-exponential with a non-zero end point gives a refolding time constant (50 ms, solid line in Figure 6B) which is identical to that from the stopped-flow experiment. The amplitude of the refolding phase is about 65%.

Disagreement between Equilibrium and Kinetics When Using GuHCl. In contrast to the above results in urea, results from experiments in which GuHCl was used show a significant difference between equilibrium and kinetic measurements of stability. At 25 °C, equilibrium fluorescence obtained in GuHCl (Figure 7A) results in the same ΔG value as for urea titrations (9.8 ± 0.1 kcal/mol, Table 1). However, stopped-flow estimates of stability and the m value using GuHCl are quite different from corresponding equilibrium values. For example, fitting the data of Figure 7B results in a $\Delta G_{kin}(0)$ of 5.5 ± 0.2 kcal/mol and an m_{kin} of 2.5 ± 0.1 kcal/mol. Moreover, the unfolding rates seem to depend on the initial environment of the folded protein (Figure 7C). In general, protein samples equilibrated in higher initial GuHCl concentrations tend to show faster unfolding. The amplitude of fluorescence change upon refolding is about 80% of that during unfolding; however, the amplitudes decrease slightly at both low and high extremes of final GuHCl concentrations (Figure 7D). In addition, there is significant nonlinearity of the dependence of ln(k) with final GuHCl concentration

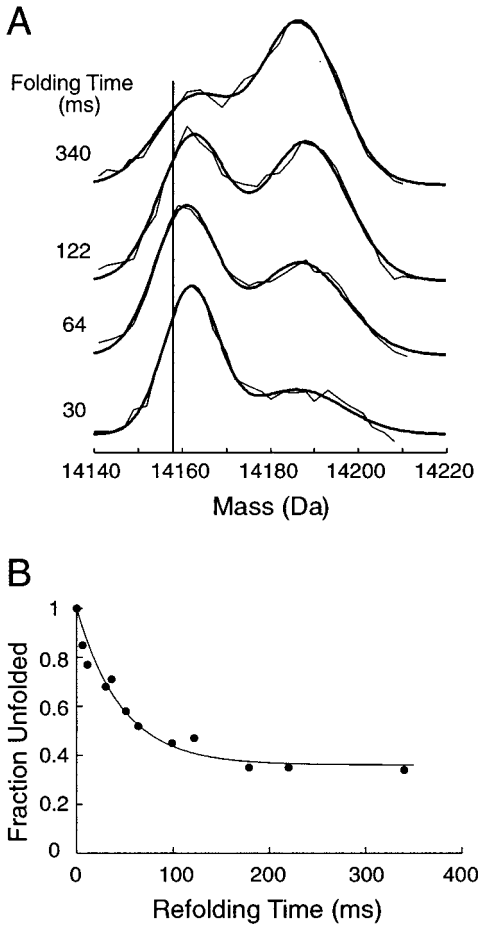

FIGURE 6: Quenched-flow followed by mass spectrometry. Refolding in 2.4 M urea, at 21 °C. (A) Example mass spectra of samples representing deuteration at different refolding times. The solid vertical line shows the peak position for 100% protonated protein. Smooth lines represent the double-Gaussian fits to the raw data (nonsmooth lines). (B) Time course of conversion from unprotected (unfolded) to protected protein populations during refolding. The *Y*-axis depicts the fraction of the population which is unfolded at the given refolding time point. The line shows fitting of the data to a single-exponential equation with a non-zero end point.

(Figure 7B) when the GuHCl concentration is >4 M. All of the above data show that villin 14T does not fold in a two-state manner in GuHCl, in contrast to the behavior in urea at 37 °C.

Quenched-Flow Experiments Using GuHCl. To detect if stable hydrogen-bonded structure occurs in the intermediate, refolding of villin 14T in 1.5 M GuHCl is monitored using quenched-flow followed by NMR and mass spectrometry. As with urea, refolding traces show single-exponential kinetics. The average refolding amplitude is about 75% of the total proton signal. The remaining 25% of the proton signal does not become protected during the 340 ms maximum folding delay of this experiment (Figure 8A). An example (residue 47) is depicted in Figure 8A. Figure 8B shows the resulting folding time constants for all residues with slow amide exchange from the native state. The average time constant is 50 ms. The stopped-flow fluorescence experiment also reveals a 50 ms refolding time constant in 1.5 M GuHCl. With a few exceptions, all of the time constants are within the range of 40−60 ms. Residues 83 and 108 show extreme time constant values (Figure 8B). Residue 98 also seems to be an outlier, but its time constant

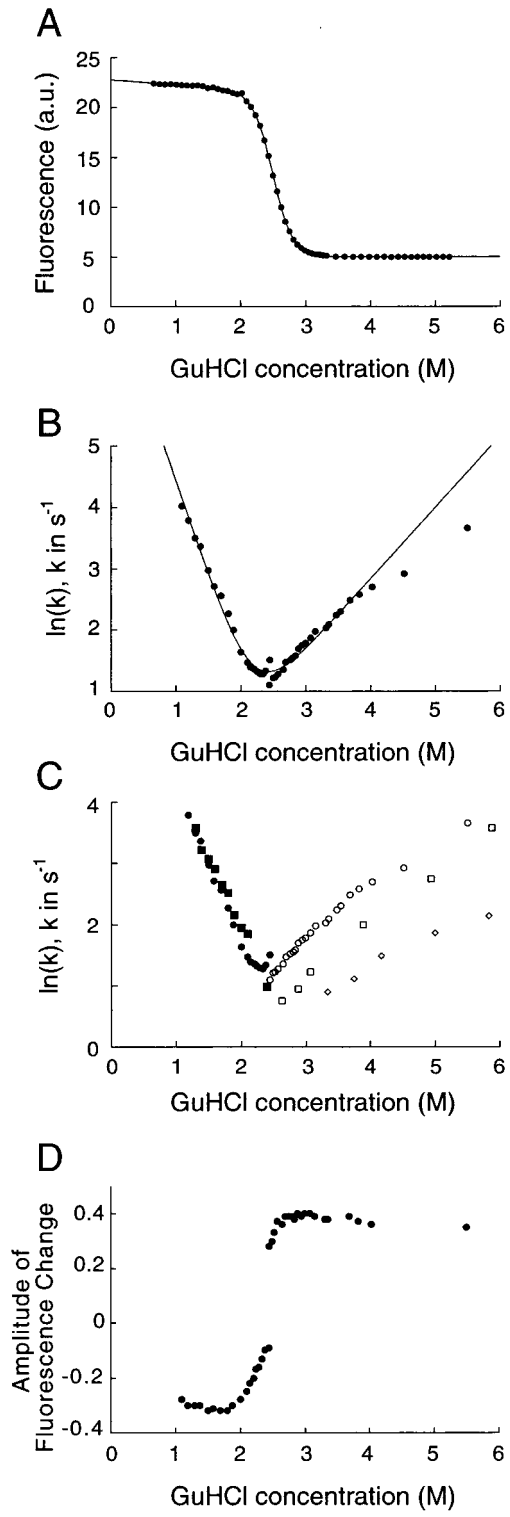

FIGURE 7: Equilibrium and stopped-flow data in GuHCl. (A) Equilibrium fluorescence titration, at 25 °C. (B) Stopped-flow fluorescence in GuHCl at 25 °C, in ln(*k*) vs denaturant concentration plots. Unfilled symbols represent refolding data, and filled symbols represent unfolding data. Only data points between 1 and 3.7 M urea were used to fit the data (to the same equation as in Figure 4). (C) Stopped-flow fluorescence at 25 °C, under different initial conditions. Unfilled circles show unfolding, with protein pre-equilibrated at 2 M GuHCl; unfilled squares show unfolding from 1.5 M GuHCl, and unfilled diamonds show unfolding from 0 M GuHCl. All refolding experiments (filled symbols) were performed with protein initially equilibrated in 4 M GuHCl. (D) Fluorescence change during refolding and unfolding as a function of final GuHCl concentration.

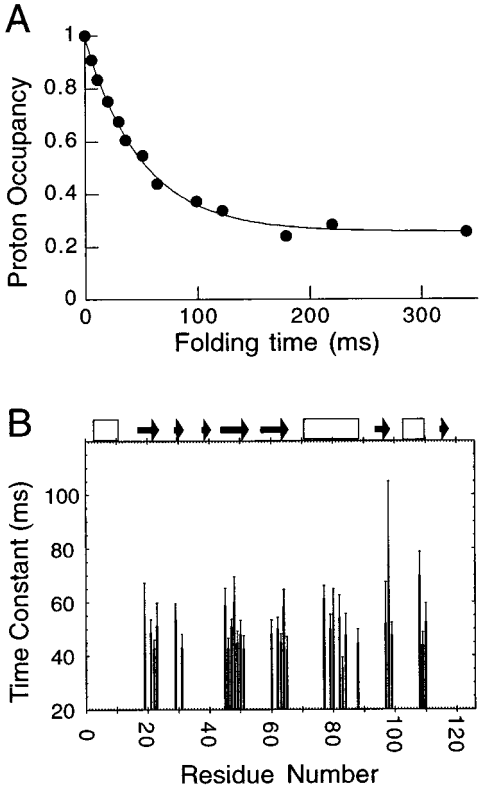

FIGURE 8: Quenched-flow followed by NMR, in 1.5 M GuHCl, at 21 °C. (A) Representative time course of protection of a single amide proton during refolding (residue 47). The solid line shows the single-exponential fit to the data. (B) Time constant (in milliseconds) of refolding as a function of residue number. Amides with slow exchange from the native state occur in residues 19, 21−23, 29, 31, 45−51, 60, 62−65, 77, 79, 80, 82−84, 88, 97−99, and 108−110. Secondary structure elements are indicated above the graph; boxes are helices, and arrows are β-strands.

has a large error. Residue 108 is located in the short α-helix adjacent to the aromatic hydrophobic core, while residue 83 is located in the long α-helix on the other side of the β-sheet. It is difficult to identify a folding intermediate on the basis of the location of these two residues; it is more likely that the rate constant errors have been underestimated in these cases.

To see if a hydrogen-bonded intermediate can be more easily detected at a lower final urea concentration, refolding of villin 14T was also monitored by quenched-flow with MS at 0.5 M GuHCl and 1 μM villin 14T. These conditions result in a single refolding phase (amplitude $\sim$ 80%), with a time constant of 5 ms (data not shown), which corresponds to the time constant obtained by extrapolation of the stopped-flow data at low GuHCl concentrations to 0.5 M. Therefore, no stably hydrogen-bonded intermediate is detected at 0.5 M GuHCl. However, when the quenched-flow experiments with MS and NMR are repeated at a higher protein concentration (40 μM), a biphasic refolding time course for all interior amides results, with each phase having about equal amplitudes (data not shown). The fast phase of refolding occurs with a τ of 5 ms; the slow phase constant is 50−100 ms. The appearance of the slow phase at higher protein concentrations suggests that it is the result of transient aggregation, as has been observed for other proteins (*41*).

Quenched-flow followed by mass spectrometry also shows that there is no detectable hydrogen-bonded refolding

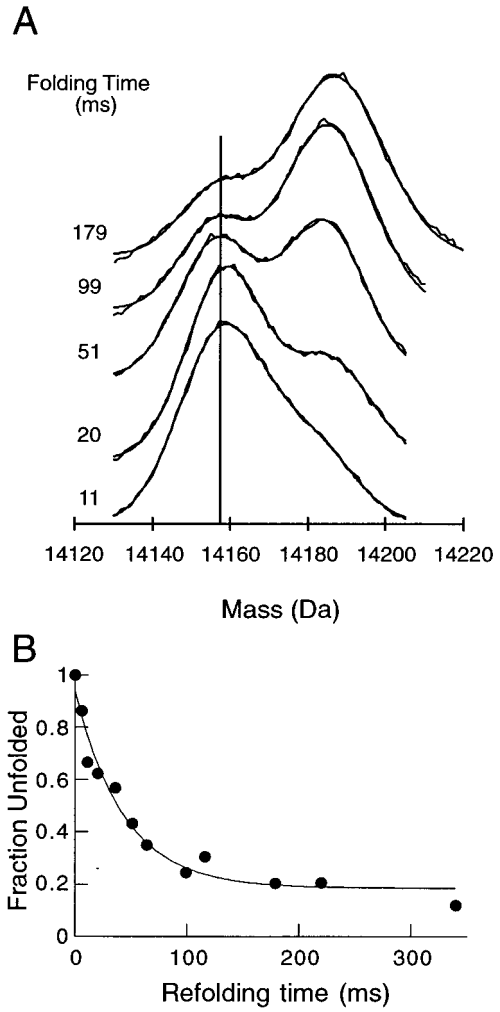

FIGURE 9: Data from quenched-flow with MS in 1.5 M GuHCl, at 21 °C. (A) Mass spectra of samples allowed to refold for different times (indicated at left) before exchange. The solid vertical line shows the peak position corresponding to fully protonated protein, and the smooth curve represents the fit of the data to a double-Gaussian equation. (B) Fraction unfolded as a function of time, as determined by integrating the double-Gaussian curves which were fitted to mass spectra of Figure 6A. The solid line shows the fit of the data to a single-exponential curve with a non-zero end point.

intermediate at 1.5 M GuHCl. The data in Figure 9A show the two peaks corresponding to the unfolded and folded proteins, at 14 159 and 14 185 Da, respectively. As before, these peaks are closely fitted by double Gaussians, suggesting that no intermediate population exists. Integration of the fitted double-Gaussian curves results in 9B. The refolding time constant is 50 ms (solid line in Figure 9B), the same value that was seen in quenched-flow with NMR and stopped-flow. The amplitude of the refolding phase is about 80%, which is also similar to the amplitudes from the other experiments.

DISCUSSION

The aim of this work is to characterize the folding pathway for villin 14T, under several experimental conditions. The results above indicate that the folding behavior of this domain is sensitive to temperature and choice of denaturant, involving a refolding intermediate at 25 °C with urea, apparent two-state folding at 37 °C with urea, and a kinetic intermediate at 25 °C with GuHCl.

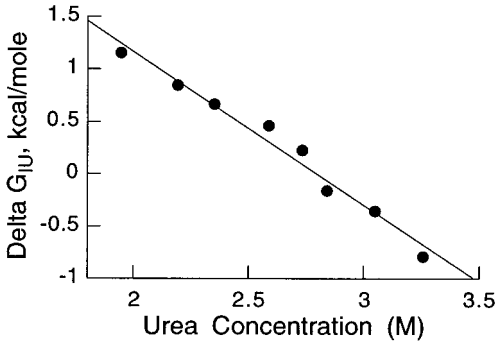

FIGURE 10: Free energy difference between the intermediate and unfolded states, as a function of urea concentration. This graph was generated assuming the reaction mechanism shown in the Discussion. See the Discussion for an explanation.

Apparent Two-State Folding at 37 °C, but Not at 25 °C. There are three criteria for demonstrating two-state folding of a protein (*20*). First, equilibrium and kinetic estimates of protein stability (ΔG) must agree. In the case of urea-unfolded villin 14T, this criterion is met at both 25 (only above 3.4 M urea) and 37 °C. At 25 °C, $\Delta G \approx 9.7$ kcal/mol, while at 37 °C, $\Delta G \approx 6.0$ kcal/mol. Second, the estimates of m values from equilibrium and kinetic measurements must match; that is, $m_{equil} = m_u - m_f$. At 25 °C, equilibrium and kinetic experiments on villin 14T both indicate $m \approx 2.2$ kcal mol^{-1} M^{-1} within the range of 3.4−7.0 M urea, while at 37 °C, $m \approx 1.6$ kcal mol^{-1} M^{-1} at all observed urea concentrations. Last, the ln(k) versus denaturant concentration plots must be linear all the way to the low and high extremes of denaturant concentration. For villin 14T at 25 °C, the ln(k) versus denaturant concentration plot is linear near the transition region, but deviates from two-state folding at low (<3.4 M) urea concentrations. At 37 °C, the stopped-flow chevron is linear throughout the range of observed denaturant concentrations (1.3−7.3 M). The refolding constants extrapolated to 0 M urea give a $\tau_f(0)$ of ≈1 ms, which is within the range of time constants measured for other two-state folding systems. Therefore, villin 14T follows the two-state model in limited regions of urea concentration at 25 °C (3.4−7 M), while at 37 °C, it folds in a two-state fashion at all observed urea concentrations.

Characterization of the Intermediate at 25 °C. At 25 °C and low final urea concentrations, villin 14T deviates from two-state behavior. One possible explanation is the establishment of a pre-equilibrium between the unfolded state (U) and an intermediate (I), which is achieved before the dead time of the kinetic experiments, and before folding to the native state (N) (*23*). Since the U-to-I transition is too fast to observe, it is impossible to distinguish whether I is a trap or an obligatory intermediate, but here it will be assumed that I is a trap. (If I is assumed to be an obligatory intermediate, the resulting values of Figure 10 depict $-\Delta G_{IU}$ instead of ΔG_{IU}.)

$$\{\mathrm{I} \overset{K_{IU}}{\rightleftharpoons} \mathrm{U}\} \xrightarrow{k_f} \mathrm{N}$$

where $K_{IU} = [U]/[I]$ and k_f is the U-to-N folding rate constant. Since U and I seem to equilibrate before the dead time of mixing, the apparent folding rate during the experiment would be k_{app} ([I] + [U]) (*23*, *42*). The above mechanism suggests that the folding rate should also be k_f[U]. Equating

the two, one obtains $k_{app} = k_f K_{IU}/(K_{IU} + 1)$. Using the measured refolding rate constants as k_{app} values, and the rates expected from the two-state model as k_f's, one can calculate K_{IU} from the previous equation. Figure 10 shows $\Delta G_{IU} = -RT \ln(K_{IU})$ as a function of urea concentration, determined from this model. If these data are fitted to a straight line and extrapolated to 0 M urea, $\Delta G_{IU}(0) = 4.1 \pm 0.3$ kcal/mol. The $\Delta G_{IU}(0)$ value is about half the free energy difference between unfolded and folded states. The slope of the linear dependence of ΔG_{IU} on urea concentration is 1.5 ± 0.1 kcal mol^{-1} M^{-1}. The ratio of this value with the *m* value obtained from equilibrium fluorescence titration is 65%, suggesting that the solvent-accessible surface area buried upon intermediate formation is about 65% of the total surface area buried during refolding. Extensive surface area burial in the intermediate corresponds with the decreasing stopped-flow amplitudes at lower urea concentrations, which indicates tryptophan burial in the intermediate.

Although the above calculation implies extensive surface area burial upon intermediate formation, the quenched-flow experiments suggest that the intermediate involves no stabilized hydrogen bonds. One can estimate the minimum stability of the hydrogen bonds that can be detected with this technique. The ratio of the exchange pulse length (20 ms) to the time constant of exchange for a random coil amide at pH 9.3 (0.6 ms) gives the minimum protection factor (PF = 33) that can be detected by the quench-flow experiment (*43*). The protection factor, defined as the ratio of the exchange rate constant of an amide in a random coil to the rate constant of the amide in the structure of interest, indicates the degree of protection of the structured amide from exchange. One can also estimate the maximum protection factor for a hydrogen-bonded amide in state I, taking into account the U-to-I equilibrium constant (Figure 10) and assuming an EX2 mechanism for exchange:

$$\{\mathrm{I{-}N_iD} \overset{K_{IU,i}}{\rightleftharpoons} \mathrm{U{-}N_iD}\} \xrightarrow{k_{ex}} \mathrm{U{-}N_iH}$$

where $I-N_iD$ is the intermediate state with the *i*th amide deuterated and protected and $U-N_iD$ is any state which has unfolded enough to expose this amide to exchange so that it can become protonated ($U-N_iH$). $K_{IU,i}$ is the equilibrium constant for local opening of the intermediate structure to allow this amide to exchange. Under EX2, the observed exchange rate constant would be $K_{IU,i}k_{ex}$ (*44*); the resulting protection factor would be $k_{ex}/(K_{IU,i}k_{ex}) = 1/K_{IU,i}$. $K_{IU,i}$ must be greater than the equilibrium constant for the I-to-U transition (K_{IU}); therefore, the maximum protection factor possible with this scheme would be $1/K_{IU}$. During the exchange pulse (at 1.25 M urea in Figure 10), $\Delta G_{IU} = 2.26$ kcal/mol, so $1/K_{IU} = 48$. Thus, the quench-flow experimental conditions are sensitive enough to detect the protection of amides which exchange with solvent only when the entire intermediate unfolds. Further work will modify the quench-flow experiment to detect protection factors greater than 10.

Since the data indicate that the intermediate contains no stable hydrogen bonds, but includes significant burial of solvent-accessible surface area and tryptophan side chains, it could involve nonspecific hydrophobic collapse of the unfolded state upon dilution of denaturant. The degree of hydrophobic collapse would increase with decreasing final urea concentration. An increased degree of hydrophobic collapse could favor a misfolded topology in a fraction of the folding molecules, perhaps by excluding the hydrophilic backbone groups in the central β-sheet from the protein core. Sosnick et al. (*45*) have also proposed that nonspecific hydrophobic collapse upon dilution of the denaturant accounts for the burst phase intermediate observed in the refolding of cytochrome *c*.

The temperature dependence of intermediate stability may also help to characterize its structure. The refolding intermediate of villin 14T is destabilized relative to the transition state at higher temperatures, and stabilized at lower temperatures. However, if the intermediate consists of nonspecific hydrophobic collapse, one would expect the opposite temperature dependence, since the hydrophobic effect generally becomes more pronounced with increasing temperature (*46*, *47*). For example, ubiquitin shows destabilization of its refolding intermediate at lower temperatures, in agreement with the hypothesis of a hydrophobically collapsed intermediate (*27*). This contradiction can be resolved by considering that the hydrophobic effect is stronger at increased temperatures for aliphatic residues, but weaker at higher temperatures for aromatic residues (*48*). Villin 14T has a higher aromatic residue content than ubiquitin. The hydrophobic cores of villin contain 20 (core 1) and 60% (core 2) aromatic residues. Together, villin's hydrophobic cores are 37% aromatic. In contrast, the ubiquitin hydrophobic core contains one aromatic residue (F45) out of a total 16. Therefore, the differential aromatic residue content of the villin14T and ubiquitin could explain the contrasting temperature dependence of the stability of their hydrophobically collapsed intermediates.

Implications of Apparent Two-State Folding at 37 °C. All single domains which have been previously shown to follow the two-state model contain a single, central hydrophobic core. Most previous studies on larger domains with compound core elements, such as ribonuclease A and dihydrofolate reductase, reveal refolding intermediates (*6*, *8*). As a result, some authors have suggested that two-state folding is the property only of small domains with single hydrophobic cores, with more complex folding behavior expected as the protein length increases (*24*). However, there is already some evidence for two-state folding of longer polypeptides. Mutant I96A of barnase shows nearly two-state folding (*28*). A two-state folding pathway has also been shown for lysozyme, existing in parallel with the originally identified, intermediate-containing pathway (*9*, *11*, *16*). However, lysozyme contains two domains, each with a single hydrophobic core; therefore, this protein would not be a good model for studying single domains with several buried structures. The kinetic results at 37 °C show the first example of apparent two-state folding for a domain with a compound core. Villin 14T is also the longest polypeptide shown so far to fold in a two-state manner.

Several studies of apparent two-state folding systems have concentrated on characterizing the activation barrier. Authors propose that the activated state consists of a partly formed hydrophobic core and little to no secondary structure (*49*−*51*). Point mutation studies of chymotrypsin inhibitor 2 (CI2) (*50*) and P22 arc repressor (*49*) show that their hydrophobic cores are loosely structured in the transition state. In addition

to loose core formation, a few specific hydrophobic contacts in CI2 seem to be more strongly formed in the activated state. Studies suggest that secondary structure formation does not contribute to the high energy of the transition state. For example, when the α-helical propensity of the GCN4 dimer is altered by point mutation, the kinetics of refolding is largely unaffected (*51*).

Therefore, hydrophobic core formation seems to be the dominant property of the transition state for fast folding proteins. However, this observation may result from the fact that most proteins with two-state folding have a single, centrally located hydrophobic core. Domains with multiple hydrophobic cores or buried secondary structures may show different transition state properties. Since most of the proteins with compound core elements have prominent folding intermediates, transition state analysis is difficult for these proteins. For example, the refolding pathway of the 126-residue domain CheY contains an intermediate; therefore, the transition state for folding is mostly inferred by characterizing the transition state for unfolding, assuming that these are identical (*3*). Analysis of the transition state for villin 14T at 37 °C would be useful in understanding the role of hydrophobic collapse in folding of domains with complex core structures.

Ratio of Kinetic and Equilibrium m Values. The ratio $-m_f/m$ roughly indicates the protein surface area buried upon going from the unfolded to the transition state, expressed as a fraction of the total surface area buried upon refolding. At 25 °C, this value is ≈86%, while at 37 °C, it is ≈74%. These figures suggest that the transition state is very similar to the native state, with respect to solvent exposure. This result is consistent with $-m_f/m$ values from studies of other two-state folding proteins.

Lack of Two-State Folding in GuHCl. Kinetic studies of villin 14T in GuHCl illustrate a point which is already clear from the urea experiments: the folding behavior is highly dependent on solvent conditions. The ln(k) versus denaturant concentration plots in GuHCl yield low $\Delta G_{kin}(0)$ values, from 4 to 5.5 kcal/mol, compared to a $\Delta G_{equil}(0)$ of 9.8 kcal/mol. Similarly, m_{kin} (2.5 ± 0.1 kcal mol^{-1} M^{-1}) is also too low compared to m_{equil} (3.93 ± 0.03 kcal mol^{-1} M^{-1}). Work to explain the different behavior of villin 14T in urea versus GuHCl is ongoing. The main difference between the two denaturants is ionic strength. The high ionic strength during GuHCl kinetic experiments could affect the relative energies of the unfolded, transition, and native states by screening strong electrostatic interactions. Equilibrium studies of CheY and RNase A show that the ionic strength of GuHCl affects thermal stability (*29*, *52*). The Mg-binding site of CheY may interact with the GuH^+ ion, stabilizing the protein. In addition, when the stabilities of variously charged coiled coils are measured using GuHCl and urea, varying electrostatic contributions to stability can be differentiated using urea, while GuHCl tends to screen charge−charge interactions and therefore shows no difference in stability between the different coiled coils (*53*). In the case of villin 14T, there are two regions where charged groups are relatively buried, whose interaction energies may be differentially shielded in the different protein states. Histidine 62 is positively charged at experimental pH (4.1), and is located very close to the aromatic hydrophobic core. Also, the stronger Ca^{2+} binding site (comprising residues E24, D43, and E73) contains several negatively charged residues which are located in a somewhat recessed part of the protein. The HSQC's of the native protein in 0.25−1.7 M GuHCl do not show any shift in the amide N−H peaks of these residues, suggesting that these regions are not shielded by GuHCl in the native state. If it is assumed that the unfolded state energy is not affected by the ionic strength of GuHCl, it is possible that the shielding effect of GuHCl would act mainly on intermediates or transition states.

Conclusion. It is shown here that villin 14T folds in an apparent two-state manner in urea at 37 °C. This is the first example of two-state folding for a domain with a compound core structure, containing two hydrophobic cores and a buried, central β-sheet. However, this two-state folding behavior is highly dependent on the temperature and choice of denaturant. A refolding intermediate is detectable at 25 °C, or if the denaturant is changed to GuHCl (at 25 °C). Evidence shows that the intermediate involves the burial of tryptophan side chains but no stable hydrogen bonding. Future work to identify the transition state for this protein at 37 °C and in urea will elucidate the role of hydrophobic collapse in nucleating folding.

ACKNOWLEDGMENT

We thank Bob Sauer and Peter Kim for use of their equipment and Dennis Rentzeperis, Greg Heffron, and Matthew Footer for help in obtaining the data.

REFERENCES

1. Anfinsen, C. B., Haber, E., Sela, M., and White, F. H. (1961) *Proc. Natl. Acad. Sci. U.S.A. 47*, 1309−1314.
2. Levinthal, C. (1968) *J. Chem. Phys. 65*, 44−45.
3. Lopez-Hernandez, E., and Serrano, L. (1996) *Folding Des. 1*, 43−55.
4. Shastry, M. C., and Udgaonkar, J. B. (1995) *J. Mol. Biol. 247*, 1013−1027.
5. Wildegger, G., and Kiefhaber, T. (1997) *J. Mol. Biol. 270*, 294−304.
6. Jones, B. E., and Matthews, C. R. (1995) *Protein Sci. 4*, 167−177.
7. Varley, P., Gronenborn, A. M., Christensen, H., Wingfield, P. T., Pain, R. H., and Clore, G. M. (1993) *Science 260*, 1110−1113.
8. Udgaonkar, J. B., and Baldwin, R. L. (1988) *Nature 335*, 694−699.
9. Khorasanizadeh, S., Peters, I. D., and Roder, H. (1996) *Nat. Struct. Biol. 3*, 193−205.
10. Matouschek, A., Serrano, L., and Fersht, A. R. (1992) *J. Mol. Biol. 224*, 819−835.
11. Dobson, C. M., Evans, P. A., and Radford, S. E. (1994) *Trends Biochem. Sci. 19*, 31−37.
12. Weissman, J. S., and Kim, P. S. (1991) *Science 253*, 1386−1393.
13. Elove, G. A., Bhuyan, A. K., and Roder, H. (1994) *Biochemistry 33*, 6925−6935.
14. Baldwin, R. L. (1996) *Folding Des. 1*, R1−R8.
15. Heidary, D. K., Gross, L. A., Roy, M., and Jennings, P. A. (1997) *Nat. Struct. Biol. 4*, 725−731.
16. Kiefhaber, T. (1995) *Proc. Natl. Acad. Sci. U.S.A. 92*, 9029−9033.
17. Kuszewski, J., Clore, G. M., and Gronenborn, A. M. (1994) *Protein Sci. 3*, 1945−1952.
18. Alexander, P., Orban, J., and Bryan, P. (1992) *Biochemistry 31*, 7243−7248.
19. Villegas, V., Azuaga, A., Catasus, L., Reverter, D., Mateo, P. L., Aviles, F. X., and Serrano, L. (1995) *Biochemistry 34*, 15105−15110.

20. Jackson, S. E., and Fersht, A. R. (1991) *Biochemistry 30*, 10428−10435.
21. Kragelund, B. B., Robinson, C. V., Knudsen, J., Dobson, C. M., and Poulsen, F. M. (1995) *Biochemistry 34*, 7217−7224.
22. Huang, G. S., and Oas, T. G. (1995) *Biochemistry 34*, 3884−3892.
23. Schonbrunner, N., Koller, K. P., and Kiefhaber, T. (1997) *J. Mol. Biol. 268*, 526−538.
24. Viguera, A. R., Martinez, J. C., Filimonov, V. V., Mateo, P. L., and Serrano, L. (1994) *Biochemistry 33*, 2142−2150.
25. Jackson, S. E., el Masry, N., and Fersht, A. R. (1993) *Biochemistry 32*, 11270−11278.
26. Shakhnovich, E., Abkevich, V., and Ptitsyn, O. (1996) *Nature 379*, 96−98.
27. Khorasanizadeh, S., Peters, I. D., Butt, T. R., and Roder, H. (1993) *Biochemistry 32*, 7054−7063.
28. Matouschek, A., and Kellis, J. T. (1990) *Nature 346*, 440−445.
29. Munoz, V., Lopez, E. M., Jager, M., and Serrano, L. (1994) *Biochemistry 33*, 5858−5866.
30. Creighton, T. E. (1994) *Nat. Struct. Biol. 1*, 135−138.
31. Sosnick, T. R., Mayne, L., Hiller, R., and Englander, S. W. (1994) *Nat. Struct. Biol. 1*, 149−156.
32. Sosnick, T. R., Mayne, L., and Englander, S. W. (1996) *Proteins: Struct., Funct., Genet. 24*, 413−426.
33. Matsudaira, P. T., and Burgess, D. R. (1982) *J. Cell Biol. 92*, 648−656.
34. Markus, M. A., Nakayama, T., Matsudaira, P., and Wagner, G. (1994) *Protein Sci. 3*, 70−81.
35. Markus, M. A., Matsudaira, P., and Wagner, G. (1997) *Protein Sci. 6*, 1197−1209.
36. Doering, D. S., and Matsudaira, P. (1996) *Biochemistry 35*, 12677−12685.
37. Pace, C. N. (1986) *Methods Enzymol. 131*, 266−280.
38. Miranker, A., Robinson, C. V., Radford, S. E., Aplin, R. T., and Dobson, C. M. (1993) *Science 262*, 896−900.
39. Myers, J. K., Pace, C. N., and Scholtz, J. M. (1995) *Protein Sci. 4*, 2138−2148.
40. Jackson, S. E., and Fersht, A. R. (1991) *Biochemistry 30*, 10436−10443.
41. Silow, M., and Oliveberg, M. (1997) *Proc. Natl. Acad. Sci. U.S.A. 94*, 6084−6086.
42. Szabo, Z. G. (1969) *Comprehensive Chemical Kinetics 2*, 24−26.
43. Connelly, G. P., Bai, Y., Jeng, M. F., and Englander, S. W. (1993) *Proteins 17*, 87−92.
44. Englander, S. W., and Kallenbach, N. R. (1983) *Q. Rev. Biophys. 16*, 521−655.
45. Sosnick, T. R., Shtilerman, M. D., Mayne, L., and Englander, S. W. (1997) *Proc. Natl. Acad. Sci. U.S.A. 94*, 8545−8550.
46. Cantor, C. R., and Schimmel, P. R. (1980) *Biophysical Chemistry, Part 1: The Conformation of Biological Macromolecules*, W. H. Freeman and Co., New York.
47. Privalov, P. L., and Gill, S. J. (1988) *Adv. Protein Chem. 39*, 191−234.
48. Tanford, C. (1980) *The hydrophobic effect: formation of micelles and biological membranes*, 2nd ed., Wiley-Interscience, New York.
49. Milla, M. E., Brown, B. M., Waldburger, C. D., and Sauer, R. T. (1995) *Biochemistry 34*, 13914−13919.
50. Itzhaki, L. S., Otzen, D. E., and Fersht, A. R. (1995) *J. Mol. Biol. 254*, 260−288.
51. Sosnick, T. R., Jackson, S., Wilk, R. R., Englander, S. W., and Degrado, W. F. (1996) *Proteins: Struct., Funct., Genet. 24*, 427−432.
52. Mayr, L. M., and Schmid, F. X. (1993) *Biochemistry 32*, 7994−7998.
53. Monera, O. D., Kay, C. M., and Hodges, R. T. (1994) *Protein Sci. 3*, 1984−1991.
54. Kraulis, P. (1991) *J. Appl. Crystallogr. 24*, 946−950.

BI980889K